Chip-based microcavities coupled to nitrogen-vacancy centers in single crystal diamond

Paul E. Barclay,[a] Kai-Mei C. Fu, Charles Santori, and Raymond G. Beausoleil
Hewlett-Packard Laboratories, 1501 Page Mill Road, Palo Alto, California 94304, USA

(Received 14 August 2009; accepted 21 October 2009; published online 12 November 2009)

Optical coupling of nitrogen-vacancy centers in single-crystal diamond to an on-chip microcavity is demonstrated. The microcavity is fabricated from a hybrid gallium phosphide and diamond material system and supports whispering gallery mode resonances with spectrometer resolution limited $Q > 25\,000$. © *2009 American Institute of Physics*. [doi:10.1063/1.3262948]

An outstanding challenge in creating solid state cavity QED systems[1] useful for quantum information processing is efficient optical coupling to high quality spin qubits.[2] The nitrogen-vacancy (NV) center in diamond is a promising candidate qubit, as it allows optical readout of long-lived single electron[3] and nuclear[4–6] spins. Using coherent optical control,[7] it may be possible to generate single photons[8,9] entangled with a single NV spin.[2,10] Chip-based nanophotonic devices, such as microcavities, can play an important role in these experiments, providing efficient optical coupling through Purcell-enhanced qubit-photon interactions and scalable optical integration of multiple qubits. Studies of optical coupling between NVs in diamond nanocrystals and high-Q dielectric microcavities[11–13] have been limited by the relatively poor nanocrystal NV optical properties, and NVs have not been observed in nanocrystalline diamond microcavities.[14,15] The alternative, nanophotonic coupling to high quality NVs in single crystal diamond, is challenging, owing to the difficulty in realizing waveguiding structures from bulk diamond.

Here we report the demonstration of high-Q microcavities fabricated in single crystal diamond by integrating a patterned high-index waveguiding layer on a diamond substrate, from which photons couple evanescently to NVs close to the diamond surface. This approach was first studied in Ref. 16, where waveguides patterned in a gallium phosphide film (GaP, $n_{\mathrm{GaP}}=3.25$) were optically coupled to NVs in a diamond substrate ($n_{\mathrm{dia}}=2.42$). Evanescent coupling was also used in Ref. 17, where an SiO_2 microsphere cavity was coupled to NVs in a diamond pillar.[18] In this letter, we measure coupling between microcavities *on-chip* and NV centers in a diamond substrate. The monolithic, chip-based nature of these devices is amenable to fabrication of more complicated nanophotonic structures such as photonic crystal nanocavities and waveguides.[19] The microcavity Q demonstrated here shows that it will be possible to efficiently collect NV spontaneous emission with proposed hybrid diamond-GaP photonic crystal devices.[19]

The devices studied here consist of GaP microdisks supported by a single crystal diamond substrate; a scanning electron microscopy (SEM) image of a device is shown in Fig. 1(a). To reduce radiation loss into leaky substrate modes, the sidewalls of the GaP structure are extended into the diamond. These hybrid microdisks[20] support high-Q whispering gallery modes, which interact evanescently with the diamond substrate. Figures 1(b) and 1(c) show cross sections of the electric field of the lowest order whispering gallery modes with dominantly radial (TE) and vertical (TM) electric field polarization, calculated using finite difference time domain (FDTD) simulations with $e^{im\phi}$ azimuthal field variation.[21] These modes are labeled TE_0^m and TM_0^m, indicating a single maximum in the radial dimension and azimuthal quantum number m.

Two hybrid diamond-GaP microdisk samples were fabricated, as summarized in Table I. NVs were created within ~200 nm of the diamond surface using N^+ ion implantation, followed by a 1 h, 950 °C hydrogen-argon anneal.[22–24] The diamond samples were then cleaned in a $H_2SO_4:KNO_3$ (20 ml:1 g, ~240 °C) solution. For fabrication of the GaP microdisks, we used a GaP layer (thickness t) grown expitaxially on an AlGaP sacrificial layer on a GaP substrate. Electron beam lithography followed by $Ar/BCl_3/Cl_2$ ECR-RIE anisotropic plasma etching and HF wet etching (7% 1:1 $HF:H_2O$) was used to define GaP microdisks supported by AlGaP pillars on a GaP substrate.[25] To transfer the microdisks to the diamond sample, a drop of HF

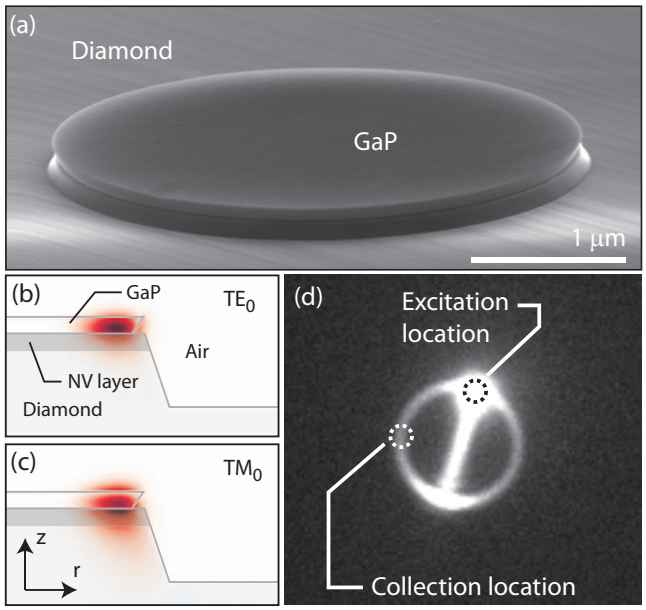

FIG. 1. (Color) (a) SEM image of a hybrid GaP-diamond microdisk. [(b) and (c)] FDTD simulated field profiles [$E_r(r,z)$ and $E_z(r,z)$, respectively], of the TE_0^m and TM_0^m modes. (d) Widefield charge-coupled device camera image of PL from a hybrid microdisk.

[a]Electronic mail: paul.barclay@hp.com.

 © 2009 American Institute of Physics

Downloaded 12 Nov 2009 to 15.243.233.68. Redistribution subject to AIP license or copyright; see http://apl.aip.org/apl/copyright.jsp

TABLE I. Hybrid microdisk sample properties. HPHT: High pressure, high temperature.

Sample	Supplier	GaP thickness, t (nm)	N^+ implantation
HPHT	Sumitomo	250	50 keV, $2\times10^{13}/cm^2$
CVD	Element 6	130	10 keV, $2\times10^{13}/cm^2$

was placed on the diamond sample surface and held by surface tension. The GaP microdisk sample was placed with its top surface facing down on the HF covered diamond surface, and held in place for 5 min. The HF completely removes the AlGaP pillars, and the GaP microdisks either fall onto the diamond surface or attach to the GaP substrate. The GaP substrate was detached from the diamond in a H_2O bath. After an N_2 drying step, a large fraction of the GaP microdisks remain attached to the diamond top surface. An anisotropic O_2 plasma ICP-RIE etch was then used to selectively remove up to 600 nm from the diamond surface not masked by the GaP structures. As discussed below and in Ref. 19, extending microdisk sidewalls into the diamond substrate allows smaller structures to be realized for a given radiation loss limited Q. Although the relative device positions are not fixed in this work, connected patterns such as integrated photonic crystal devices[19] may be compatible with this process.

Optical coupling of NV photoluminescence (PL) into microdisk modes was studied using a confocal microscope to optically excite NVs near the microdisk edge, as shown in Fig. 1(d). A green source (532 nm laser) was focused to a $\sim$0.5 μm diameter spot using a numerical aperture=0.6 microscope objective. A dichroic mirror and long wavelength pass filter (cut-on $\sim$540 nm) spectrally separated reflected laser light from the PL. The objective collected PL from a region of the microdisk edge at an azimuthal coordinate rotated $\sim$90° from the excitation spot. This spatial filtering was accomplished by focusing the collected PL through a 50 μm diameter pinhole at 37.5× magnification.

Figures 2(a) and 2(b) show typical PL spectra for hybrid microdisks from the CVD and HPHT samples, respectively. In both spectra, a broad background corresponding to emission from NV centers is visible, as evidenced by the peak at $\lambda\sim637$ nm from the NV^- zero phonon line (ZPL), and a global maximum near 680 nm from phonon assisted NV^- emission. Also visible is bulk diamond Raman emission at 572 nm. Superimposed upon this background are sharp peaks resulting from NV emission coupled into the microdisk modes, a fraction of which is then scattered or radiated into the microscope objective. The CVD device measured in Fig. 2(a) has $t\sim130$ nm, and for $\lambda>650$ nm only supports high-Q TE_0^m whispering gallery modes. The HPHT device measured in Fig. 2(b) has $t\sim250$ nm, and in addition to TE_0^m modes, supports high-Q TM_0^m, TE_1^m, and TM_1^m modes. Also visible in the spectra are low-Q oscillations resulting from Fabry–Pérot-like transverse modes, whose field distribution along the microdisk diameter (d) is evident in Fig. 1(d). The difference in measured PL intensity between Figs. 2(a) and 2(b) is a result of the higher implanted NV density of the relatively nitrogen rich HPHT sample compared to the CVD sample.

A spectrum illustrating the detailed mode structure of an HPHT hybrid microdisk is shown in Fig. 3(a). Regularly spaced sets of resonances with incrementing m numbers are

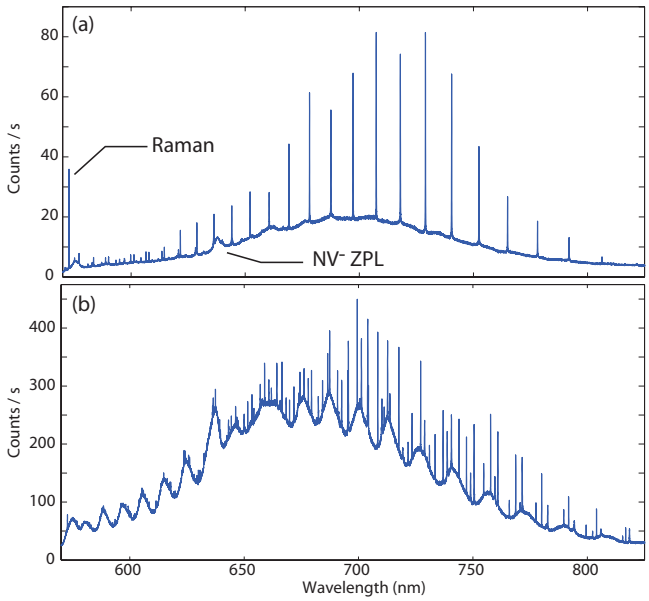

FIG. 2. (Color) PL spectra of GaP-diamond microdisks excited with a 532 nm source. Microdisk thickness and diameter $d\sim[4.6,4.5]$ μm, $t\sim[130,250]$ nm for the devices measured in (a) and (b), respectively. Diamond etch depth $h\sim600$ nm. Excitation power ~2.5 mW.

evident. The polarization and radial mode labels for a given resonance can be determined by measuring its free spectral range (FSR) as a function of wavelength, and comparing with FDTD simulated values. The results are shown in Fig. 3(b) for four families of resonances in Fig. 2(b); also shown are FDTD simulated FSR dispersion.

The largest peak in Fig. 3(a) is associated with a TM_0^m resonance and has a linewidth that is not measurably broader than the spectrometer resolution. A fit to this resonance, derived from a Lorentzian convolved with a Gaussian approximation for the system response function (calibrated using spectral lines from a Hg lamp), is shown in Fig. 3(c). The

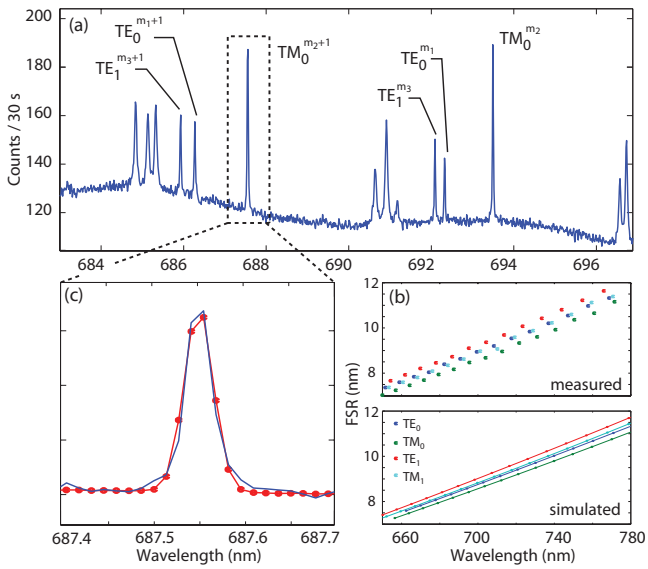

FIG. 3. (Color) (a) PL spectra of a $[t,d]=[0.25,6.5]$ μm microdisk. From FDTD simulations. we estimate that $[m_1,m_2,m_3]=[83,82,77]$. (b) Measured (top) and FDTD calculated (bottom) FSR dispersion of the four highest-Q sets of modes in Fig. 2(b). GaP refractive index dispersion (Ref. 26) was included in FDTD simulations. (c) System response limited lineshape of the TM_0^m resonance. Fit of a Lorentzian convolved with the pixelized Gaussian system response shown in red.

Downloaded 12 Nov 2009 to 15.243.233.68. Redistribution subject to AIP license or copyright; see http://apl.aip.org/apl/copyright.jsp

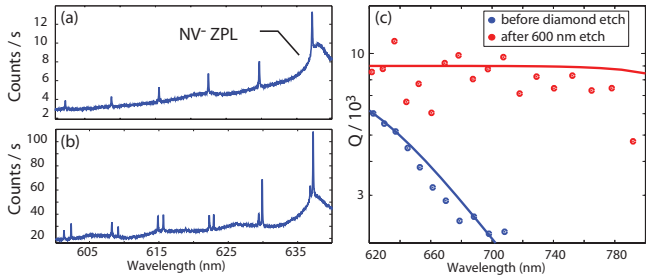

FIG. 4. (Color) Effect of diamond etching on microdisk mode spectra ($[t,d]=[0.130,4.5]$ μm). PL spectra (a) before and (b) after 250 nm vertical diamond etching. Excitation power in [(a) and (b)] ~[0.25,2.5] mW. (c) Wavelength dependence of Q for the TE-0 mode before and after 600 nm diamond etching. Simulated values for Q shown by solid lines, assuming $1/Q=1/Q_{\mathrm{rad}}+1/Q_i$ where $Q_{\mathrm{rad}}(\lambda)$ is calculated using FDTD, and $Q_i=9000$.

best-fit linewidth of the Lorentzian was smaller than the error in the measured system response, placing a lower limit of $Q>2.5\times10^4$. Two other sets of resonances in Fig. 3(a), associated with the TE_0^m and TE_1^m microdisk modes, also have linewidths close to the system resolution. An upper limit of $Q<7.5\times10^4$ for these resonances was measured by placing an adjustable interferometer at the spectrometer input to determine the coherence length of light emitted from the unresolved microdisk resonance. The GaP microdisks support resonances with $Q\sim6\times10^4$ prior to being transferred to the diamond substrate, as measured using a fiber taper to evanescently probe the microdisk modes with a tunable laser source.[25] These measurements place an upper bound on the Q of the GaP-diamond microdisk. For this device, the TM_0^m mode interacts most strongly with NVs near the diamond surface, as it has both the smallest mode volume, V, and the largest relative field strength in the diamond substrate, η.[27] From FDTD simulations, $[V,\eta]=[43,0.48]$ for a TM_0^{89} standing wave mode of this device near $\lambda=637$ nm.

Etching the diamond to extend the microdisk sidewalls into the substrate permits smaller V and larger η devices to be realized for a given radiation loss limited Q.[19] Figures 4(a) and 4(b) show spectra for a $[d,t]=[4.5,0.13]$ μm hybrid microdisk before and after the diamond etch step. Note the emergence of a second family of previously low-Q resonances (the TE_1^m modes, for this device) after etching. Prior to etching the diamond, the TE_0^m mode Q decreases exponentially for $\lambda>620$ nm due to radiation loss. After etching, the radiation loss cutoff is increased above 780 nm. This is consistent with FDTD simulated Q dispersion, as shown in Fig. 4(c), assuming that the device has an intrinsic $Q_i\sim9000$. At $\lambda\sim637$ nm, $[V,\eta]=[18,0.57]$ for the TE_0^{56} mode of this device. The relatively low Q_i, compared with that of the larger t device in Fig. 3, is a result of a lower GaP surface quality and increased surface-field interaction. The etched sidewalls have a 3 nm rms roughness (80 nm correlation length) due to suboptimal GaP etching and lithography. It is estimated that this effect limits $Q<1.7\times10^4$.[28] In addition, the GaP underside has roughness from imperfect electron-beam resist removal. These imperfections can be improved in future devices.

These results provide a proof-of-principle demonstration of on-chip nanophotonic devices for efficient NV optical coupling. The relevant cavity-QED parameters[1] for the $[d,t]=[4.5,0.13]$ μm microdisks are $[g_{\mathrm{ZPL}},\kappa,\gamma,\gamma_{\mathrm{ZPL}}]/2\pi=[0.30,26,0.013,0.0004]$ GHz. Here, g_{ZPL} is the coupling strength[19] between a single microdisk photon and the NV^- ZPL, for an NV^- optimally oriented and positioned at the diamond surface, $\kappa=\omega/2Q$ is the microdisk photon decay rate, and γ and γ_{ZPL} are the *total* and *ZPL* spontaneous emission rates of an NV^-. At low temperatures, the ZPL spontaneous emission rate of an optimally positioned NV^- into a microcavity mode is predicted to be enhanced by $F_{\mathrm{ZPL}}\sim17$. This corresponds to coupling $\beta\sim34\%$ of the total NV^- spontaneous emission (e.g., including phonon sideband emission) into the microcavity. If the Q of this device can be increased to 2.5×10^4, $F_{\mathrm{ZPL}}\sim47$ should be possible. Similarly, a photonic crystal nanocavity[19] fabricated from this material system, and supporting resonances with $Q>10^4$ as demonstrated here, will allow $\beta\rightarrow1$, and provide a platform for on-chip integration of multiple devices required by applications in quantum information processing.

P.B. thanks Oskar Painter for access to fabrication tools used in initial fabrication process development. This material is based upon work supported by DARPA under Award No. HR0011-09-1-0006 and The Regents of the University of California.

[1] H. J. Kimble, Phys. Scr. **t76**, 127 (1998).
[2] S. C. Benjamin, B. W. Lovett, and J. M. Smith, Laser Photonics Rev. **3**, 556 (2009).
[3] F. Jelezko, T. Gaebel, I. Popa, A. Gruber, and J. Wrachtrup, Phys. Rev. Lett. **92**, 076401 (2004).
[4] F. Jelezko, T. Gaebel, I. Popa, M. Domhan, A. Gruber, and J. Wrachtrup, Phys. Rev. Lett. **93**, 130501 (2004).
[5] M. V. Gurudev Dutt, L. Childress, L. Jiang, E. Togan, J. Maze, F. Jelezko, A. S. Zibrov, P. R. Hemmer, and M. D. Lukin, Science **316**, 1312 (2007).
[6] L. Childress, M. V. Gurudev Dutt, J. M. Taylor, A. S. Zibrov, F. Jelezko, J. Wrachtrup, P. R. Hemmer, and M. D. Lukin, Science **314**, 281 (2006).
[7] C. Santori *et al.*, Phys. Rev. Lett. **97**, 247401 (2006).
[8] C. Kurtsiefer, S. Mayer, P. Zarda, and H. Weinfurter, Phys. Rev. Lett. **85**, 290 (2000).
[9] A. Beveratos, S. Kuhn, R. Brouri, T. Gacoin, J.-P. Poizat, and P. Grangier, Eur. Phys. J. D **18**, 191 (2002).
[10] C. Cabrillo, J. I. Cirac, P. García-Fernández, and P. Zoller, Phys. Rev. A **59**, 1025 (1999).
[11] Y.-S. Park, A. K. Cook, and H. Wang, Nano Lett. **6**, 2075 (2006).
[12] P. E. Barclay, O. Painter, C. Santori, K.-M. Fu, and R. Beausoleil, Opt. Express **17**, 8081 (2009).
[13] S. Schietinger, T. Schroder, and O. Benson, Nano Lett. **8**, 3911 (2008).
[14] C. F. Wang, Y.-S. Choi, J. C. Lee, E. L. Hu, J. Yang, and J. E. Butler, Appl. Phys. Lett. **90**, 081110 (2007).
[15] C. F. Wang, R. Hanson, D. D. Awschalom, E. L. Hu, T. Feygelson, J. Yang, and J. E. Butler, Appl. Phys. Lett. **91**, 201112 (2007).
[16] K.-M. C. Fu *et al.*, Appl. Phys. Lett. **93**, 234107 (2008).
[17] M. Larsson, K. N. Dinyari, and H. Wang, Nano Lett. **9**, 1447 (2009).
[18] T. Babinec, B. M. Hausmann, M. Khan, Y. Zhang, J. Maze, P. R. Hemmer, and M. Loncar, arXiv:0908.0233v2.
[19] P. E. Barclay, K. M. Fu, C. Santori, and R. G. Beausoleil, Opt. Express **17**, 9588 (2009).
[20] M.-C. Tien, A. T. Ohta, K. Yu, S. L. Neale, and M. C. Wu, Appl. Phys. A: Mater. Sci. Process. **95**, 967 (2009).
[21] Available from http://ab-initio.mit.edu/wiki/index.php/Meep.
[22] G. Davies, S. C. Lawson, A. T. Collins, A. Mainwood, and S. J. Sharp, Phys. Rev. B **46**, 13157 (1992).
[23] J. Meijer *et al.*, Appl. Phys. Lett. **87**, 261909 (2005).
[24] C. Santori, P. E. Barclay, K.-M. C. Fu, and R. G. Beausoleil, Phys. Rev. B **79**, 125313 (2009).
[25] K. Srinivasan, M. Borselli, T. J. Johnson, P. E. Barclay, O. Painter, A. Stintz, and S. Krishna, Appl. Phys. Lett. **86**, 151106 (2005).
[26] D. E. Aspnes and A. A. Studna, Phys. Rev. B **27**, 985 (1983).
[27] $V=(\lambda/n_{\mathrm{GaP}})^{-3}\int n^2(\mathbf{r})|E(\mathbf{r})|^2d\mathbf{r}/(n^2(\mathbf{r}_o)|E(\mathbf{r}_o)|^2)$ and $\eta=E(\mathbf{r}|n(\mathbf{r})=n_{\mathrm{dia}})|_{\mathrm{max}}/E(\mathbf{r}_o)$, where $n^2|E|^2$ is maximized at $\mathbf{r}_o$.
[28] M. Borselli, T. J. Johnson, and O. Painter, Opt. Express **13**, 1515 (2005).

Downloaded 12 Nov 2009 to 15.243.233.68. Redistribution subject to AIP license or copyright; see http://apl.aip.org/apl/copyright.jsp